Investigation of co-transport behavior of strontium and bentonite colloids in granite disposal environment

Yang-Chun Leng[1] · Jin-Cai Feng[2] · Qiao Jiang[3] · Ze-Hua Li[1] · Hao-Xin Feng[1]

Abstract

Colloids are prevalent in nuclear waste repositories, with bentonite colloids posing an uncontrollable risk factor for nuclide migration processes. In this study, static adsorption experiments were coupled with dynamic shower experiments to comprehensively investigate the influence of bentonite colloids on Sr^{2+} migration in granite, considering adsorption capacity. Bentonite colloids have a considerably greater adsorption capacity than both bentonite and granite, with a maximum adsorption of 30.303 mg/g. The adsorption behavior of bentonite colloids on Sr^{2+} is well described by the Langmuir isotherm and pseudo-second-order kinetic models, indicating that a single-layer chemical adsorption process is controlled by the site activation energy. The adsorbed Sr^{2+} is unevenly distributed on the colloids, and the adsorption mechanism may involve ion exchange with Ca. Bentonite colloids exhibit superior adsorption in neutral environments. The cations in groundwater inhibit Sr^{2+} adsorption, and the inhibition efficacy decreases in the order $Fe^{3+} > Ca^{2+} > Mg^{2+} > K^+$. The presence of bentonite colloids in a granite column slightly influences the retention of Sr^{2+} in the column while markedly reducing the Sr^{2+} penetration time from 70 h to 18 h. However, the coexistence of Co^{2+}, Ni^{2+}, and Cs^+ in a multinuclide system weakens the ability of the colloids to promote Sr^{2+} migration. In comigration of colloid and multinuclide systems, the adsorption of nuclides by bentonite colloids causes the nuclide migration speed to decrease in the order $Sr^{2+} > Cs^+ > Ni^{2+} > Co^{2+}$. This study provides insights into Sr^{2+} migration in cave repositories for low- and medium-level radioactive waste.

Keywords Granite · Radioactive cave disposal · Bentonite colloid

1 Introduction

Low- and medium-level radioactive waste is primarily disposed near the surface. In recent years, there has been growing interest in the disposal of rock caves, to increase safety. The Chinese 14th Five-Year Plan includes provisions for constructing the first rock cave disposal facility for low- and medium-level radioactive waste in Guangdong Province. The cave repository is situated in a granite layer with four barriers to prevent nuclide migration. Gaomiaozi bentonite serves as the backfill material, with granite as the surrounding rock [1]. However, barrier systems can fail under unforeseen circumstances such as extreme weather and geological activities during long-term disposal, enabling groundwater to transport nuclides such as ^{137}Cs, ^{60}Co, ^{90}Sr, and ^{131}I into the biosphere, thereby irreversibly harming the ecological environment [2]. Among these nuclides, ^{90}Sr is a prominent fission product of radioactive waste that is known for its solubility and mobility in water [3–5]. This nuclide is highly biologically toxic and can inflict considerable damage to the bone marrow and bone tissue, increasing the risk of cancer and leukemia [6]. Therefore, close monitoring of the adsorption and migration of ^{90}Sr in repository barrier materials is essential for long-term safety assessments.

Colloids are usually particles with diameters of 1 nm to 1 μm suspended in a fluid [7]. Colloids have large specific

✉ Yang-Chun Leng
lyc@swust.edu.cn

1　School of National Defense Science and Technology, Southwest University of Science and Technology, Mianyang 621000, China

2　Yangjiang Nuclear Power Co., Ltd., Yangjiang 529500, China

3　College of Nuclear Technology and Automation Engineering, Chengdu University of Technology, Chengdu 610059, China

surface areas and charged surfaces, resulting in a high affinity for the vast majority of nuclides in repositories. The many types of colloids in the water environment of waste repositories include inorganic colloids derived from clay minerals, iron and aluminum oxides/hydroxides from the corrosion of waste containers, organic colloids formed from organic macromolecules and humic acid, and biological colloids, such as bacteria and viruses. Bentonite is used as backfill material and is abundant throughout the repository. Consequently, bentonite colloids are the primary colloidal species in nuclear waste repositories [8]. Bentonite colloids are produced by underground erosion and soaking of bentonite. However, the subsequent continuous loss of bentonite and degradation of engineering barriers [9] threaten the blocking capacity of the engineering barrier system of the repository. Bentonite colloids have large specific surface areas and can chemically adsorb or form complexes with nuclides. Thus, bentonite colloids transport nuclides, affecting the migration behavior of nuclides in the repository. Several studies have confirmed that bentonite colloids significantly affect the migration of radionuclides in repositories [10–13]. Consequently, considering the impact of bentonite colloids is crucial for assessing the security of repositories.

Granite serves as the final barrier in a repository, bridging the engineered barrier and the biosphere. Bentonite colloids transporting radionuclides through the engineered barrier come into direct contact with granite. During this interaction, bentonite colloids may be retained in the granite regardless of radionuclides, thereby penetrating the granite and enabling nuclides to be retained in the granite. Bentonite colloids affect nuclide migration in granite through a complex and reversible process, which may have different effects on different nuclides. Numerous studies have shown that the presence of bentonite colloids may diminish the ability of surrounding rock barriers to block nuclides. Katezirina et al. [14] investigated the migration behavior of ^{137}Cs on fractured granite in the presence of bentonite colloids and found that bentonite colloids transport a small portion of ^{137}Cs through the granite. Similarly, Zheng et al. [2] investigated the impact of gibbsite and sodium bentonite colloids on U(VI) transport in saturated granular granite columns. The strong binding affinity of U(VI) to the colloids enhanced U(VI) transport. However, the interactions and cotransport modes of colloids and nuclides may also inhibit or eliminate the effect of bentonite on nuclide migration in granite [15]. Elo et al. [16] conducted column experiments and showed that mobile bentonite colloids have a negligible effect on Np(V) migration in granite. By contrast, Timothy et al. [17] found that Am(III) transport by bentonite colloids is governed by the desorption of Am(III) from specific binding sites on the colloids. Bentonite colloids weakly promote Am(III) transport. Most of the numerous studies that have been performed on bentonite colloids have focused on either the adsorption properties of colloids or the direct impact of colloids on nuclide migration. However, few experiments have been conducted on joint adsorption and migration to comprehensively investigate the influence of bentonite colloids on nuclide migration in granite in terms of adsorption capacity.

Hence, in this study, strontium (Sr) was considered as the target nuclide, sampling it from the surrounding granite and backfill material (bentonite) in the first cave repository for low- and medium-level radioactive waste in China. The physical and chemical properties of granite and bentonite in the area were characterized, and bentonite colloids were produced using local groundwater. Batch adsorption experiments were performed to compare the adsorption of Sr^{2+} on bentonite colloids, bentonite, and granite. The mechanism of Sr^{2+} adsorption onto bentonite colloids was elucidated by combining empirical models with characterization methods. Accordingly, dynamic migration experiments were conducted to investigate the impact of bentonite colloids on the migration behavior of Sr^{2+} in granite columns, with a particular focus on the influence of a multinuclide system on Sr^{2+} migration. This study provides insights into accurate estimation of the potential risk of Sr migration in cave repositories for radioactive waste.

2 Materials and methods

2.1 Geological materials

Granite samples were obtained from granite rock formations near a low- and medium-level radioactive waste repository in Guangdong Province. The samples were extracted from a depth of 173 m with a specific surface area of 2.54 m^2/g. The bentonite samples were obtained from Gaomiaozi, Inner Mongolia, and had a measured specific surface area of 38.278 m^2/g. The elemental and oxide compositions of both granite and bentonite samples were determined using an Axios series X-ray fluorescence spectrometer (XRF). The findings are presented in Table 1. Groundwater samples were extracted

Table 1 Oxide mass percentage of granite and bentonite

Element (%)	SiO$_2$	Al$_2$O$_3$	K$_2$O	Fe$_2$O$_3$	CaO	Na$_2$O	MgO
Granite	67.68	10.84	8.16	5.72	5.03	0.56	0.34
Bentonite	74.02	15.56	1.82	2.31	1.25	1.50	2.86

from boreholes proximal to the cave repository at depths ranging from 148 to 173 m. During sampling, the groundwater had a flow rate of 41.5 L/min, conductivity of 298.5 µS/cm, and pH of 6.7. Groundwater samples were analyzed for major cation and anion compositions using inductively coupled plasma-mass spectrometry (ICP-MS) and ion chromatography, respectively, and the results are shown in Table 2.

2.2 Experimental instruments and materials

Transmission micrographs of the samples were obtained using field-emission transmission electron microscope (FETEM) (Libra200FE, Zeiss, Germany). Electron micrographs of the samples were obtained using a high-resolution cold-field-emission scanning electron microscopy/energy-dispersive X-ray spectroscopy (SEM-EDS) (UItra55, Zeiss, Germany). The zeta potentials (Zeta) of the samples were measured using a potentiometer (Zeta-PALS, Brookhaven, USA). The mineral compositions of the samples were determined by an X-ray diffractometer (XRD) (TD-3500, Panaco, Netherlands). The functional group compositions of the samples were determined using a Fourier transform infrared (FT-IR) absorption spectrometer (Frontier, Perkin Elmer, USA). Colloid mass concentrations were measured using a gravimetric method combined with ultraviolet (UV) spectrophotometry (V-5800, Yuanyi, China). The residual Sr^{2+} concentration in the solution was measured by ICP-MS (iCAP6500, Thermo Fisher, USA).

Hydrochloric acid (HCl) was obtained from China West Long Science Co., Ltd. (China). Sodium hydroxide (NaOH, 99%), ferric chloride ($FeCl_3$, 99%), calcium chloride ($CaCl_2$, 99%), magnesium chloride ($MgCl_2$, 99%), and potassium chloride (KCl, 99%) were obtained from Tianjin Zhiyuan Chemical Reagent Co. Ltd. (China). Caesium chloride (CsCl, > 99%) and strontium chloride hexahydrate ($SrCl_2 \cdot 6H_2O$, > 99%) were procured from Aladdin Reagent Factory (China), and cobalt chloride hexahydrate ($CoCl_2 \cdot 6H_2O$, > 99%) and nickel chloride hexahydrate ($NiCl_2 \cdot 6H_2O$, >99%) were purchased from Macklin Reagent Company (China). All chemical reagents and drugs used in this study were of analytical grade and were not further purified before use.

2.3 Preparation of bentonite colloids

Ten grams of bentonite powder (200 mesh) was weighed and dispersed in 1 L of ultrapure water with a resistivity of 18.25 MΩ m. The powder was dispersed by ultrasonic agitation for 30 min, followed by magnetic stirring for 4 h to ensure uniform mixing. The mixture was allowed to settle at room temperature for two days. The resulting sample was centrifuged at 4000 rpm for 15 min to remove particles larger than 1 µm. The separated solution was transferred to a dialysis bag for purification. The dialysis water was periodically replenished, and the pH and conductivity were monitored using pH and conductivity meters, respectively. The conductivity of the solution decreased from 160 to 10.58 µS/cm during dialysis, indicating that the colloidal dispersion had a low ionic strength and therefore an appropriate dispersion coefficient. The prepared colloidal samples were stored in a sealed conical flask at room temperature until further use. The colloidal concentration was determined by using the differential gravity method combined with UV spectrophotometry, following the method used in our previous study [18]. A colloidal sample solution with a desired concentration gradient was prepared based on the mass concentration obtained using the differential gravity method. The full spectrum of the colloidal solution was scanned using a UV-visible spectrophotometer, and the characteristic wavelength of the solution was determined to be 240 nm. The colloid mass concentration was determined by generating a standard curve ($R^2 = 0.999$) from the data.

2.4 Adsorption/desorption experiments

Batch adsorption experiments were conducted on two groups: a powder (S1) and colloidal (S2) group, to investigate the adsorption behavior of Sr^{2+} on geological barrier materials and colloids, respectively. Each experiment was repeated three times, and the average measurement was recorded. For Group S1, several portions of granite (Gt) and bentonite (Bt) powder were weighed and placed in polypropylene centrifuge tubes, to which 4.5 mL of deionized water was added. Group S2 was prepared by adding a bentonite colloidal (BC) solution to the centrifuge tubes. Samples from both groups were equilibrated overnight at room temperature. Subsequently, 4.5 mL of Sr^{2+} solution was added to each sample, to achieve the desired nuclide concentration. In experiments, 4.5 mL of a mixed solution of Sr^{2+} and the respective ions was added to the sample, to investigate the influence of specific ions on

Table 2 Chemical composition of groundwater near the cave repository

Element (mg L^{-1})	Al^{3+}	Ca^{2+}	Mg^{2+}	K$^+$	Si^{4+}	Mn^{2+}
	0.379	39.651	2.134	3.530	36.484	0.562
	Fe^{3+}	SO$_4^{2-}$	NO$_3^-$	Cl$^-$	F$^-$	–
	0.616	3.87	0.529	17.7	4.65	–

adsorption. The pH values of the samples were adjusted using trace quantities of hydrochloric acid and sodium hydroxide. The samples were placed in an oscillating box and agitated until the adsorption equilibrium was reached. The equilibrated samples were centrifuged at 10000 r/min for 30 min to separate the solid and liquid phases. The supernatant of the Group S1 samples was directly diluted, and the residual Sr^{2+} concentration was determined using ICP-MS. To ensure that the bentonite colloids were completely separated from the adsorbed solution, the supernatant of the S2 group was passed through a 0.1 μm filter membrane before the residual Sr^{2+} concentration in the liquid phase was determined. A desorption experiment was conducted after the completion of the adsorption experiment. The suspension that remained at the end of the adsorption experiment was removed to yield a granite sample with adsorbed Sr^{2+}. An equal volume of solution and pH were added to the sample and shaken under the same experimental conditions as those used for the adsorption experiment, to reach desorption equilibrium. The sample was centrifuged, filtered, and analyzed using ICP-MS to determine the Sr^{2+} concentration in the supernatant.

2.5 Migration experiment

The migration experiment was performed using a dynamic shower column with a length of 20 cm and diameter of 2.5 cm, which was filled with a soil column with an actual length of 14 cm. The experimental setup is illustrated in Fig. 1. Coarse-grained granite (60–80 mesh) was wet-filled into the shower columns. Nylon nets were placed at both the upper and lower ends of the column to prevent the granite powder from escaping the eluent during the filling process. The filled granite was continuously washed with an upward flow of ultrapure water at a constant rate until water flow equilibrium was reached in the shower column to ensure a stable moisture content throughout the experiment.
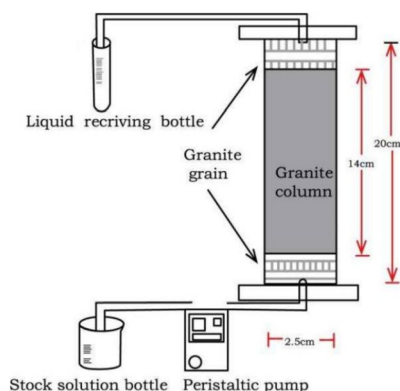

Fig. 1 (Color online) Schematic diagram of migration experimental device

The Sr^{2+} migration experiment was performed on the equilibrated shower column in two stages: transport and elution. Prior to conducting the experiment, a Sr^{2+} solution (Sr^{2+} and ionized water), BC-Sr^{2+} solution (bentonite colloid, Sr^{2+}), and mixed solution (bentonite colloids, Sr^{2+}, Cs^+, Co^{2+}, Ni^{2+}) were prepared, each with a nuclide concentration of 100 mg/L along with a bentonite colloid concentration of 250 mg/L, to simulate the expected near-field range of spent fuel storage. During the transport stage, the prepared solution was continuously added to the lower end of the granite column at a fixed flow rate of 4 mL/h via a peristaltic pump. Samples were periodically withdrawn and diluted for testing until the nuclide concentration stabilized. During the elution stage, ultrapure water was continuously pumped into the granite column at a constant flow rate of (4 mL/h). Regular sampling and testing were conducted until the simulated nuclide concentration in the detection solution approached zero.

2.6 Data analysis

The adsorption capacity for Sr^{2+}(q_e) was determined for granite, bentonite, and bentonite colloid. The migration of Sr^{2+} in the granitic media was analyzed by calculating the longitudinal diffusion coefficient (D_L), which is expressed as:

$$q_e = \frac{C_0 - C_e}{m} \times V \tag{1}$$

$$v = L/t_{0.5} \tag{2}$$

$$D_L = \frac{1}{8}\left[\frac{L - v_{t_{0.16}}}{\sqrt{t_{0.16}}} - \frac{L - v_{t_{0.84}}}{\sqrt{t_{0.84}}}\right]^2 \tag{3}$$

where C_0 and C_e are the mass concentrations of Sr^{2+} in the initial solution and at adsorption equilibrium, respectively; in mg L^{-1}, m is the mass of the sample, and g is the gravitation constant; and V is the sample volume in mL used in the adsorption experiment. v is the actual migration speed of the nuclide, m/s; L is the length of the migration column, which is 0.2 m.

2.7 Adsorption model

The adsorption data obtained at different contact times were fitted using pseudo-first-order and pseudo-second-order kinetic models and the Weber-Morris (W-M) internal diffusion model to obtain kinetic information on the mineral and colloid surface adsorption, which was subsequently used to

infer the adsorption mechanism of the sample. The kinetic models are provided below [19, 20]:

$$\frac{1}{q_t} = \frac{k_1}{q_e \cdot t} + \frac{1}{q_e} \qquad (4)$$

$$\frac{t}{q_t} = \frac{t}{q_e} + \frac{1}{q_e^2 k_2} \qquad (5)$$

$$q_t = k_{id} \times t^{\frac{1}{2}} + C \qquad (6)$$

where q_t and q_e are the unit adsorption capacity for Sr^{2+} by the sample at time t and at adsorption equilibrium, respectively, mg g^{-1}; k_1 is the pseudo-first-order rate constant, d^{-1}; k_2 is the pseudo-second-order rate constant, g (mg d)$^{-1}$; k_{id} is the W-M model rate constant, d$^{-1/2}$; and C is the influence constant of boundary layer thickness on adsorption, mg g^{-1}.

The adsorption data obtained at different Sr^{2+} concentrations were fitted using the Langmuir, Freundlich, Temkin, and Dubinin-Radushkevich (D-R) isotherm models. The Langmuir isotherm model assumes single-layer adsorption, and the attraction between molecules decreases sharply as the distance between the molecules increases. The Freundlich isotherm model is based on adsorption with an uneven distribution of sites on the adsorbent surface. The Temkin model assumes that adsorption energy decreases linearly with increasing surface coverage [21]. The D-R isotherm model can be used to calculate the average free energy of adsorption and determine the adsorption type. The model is expressed as follows [22, 23]: Langmuir:

$$q_e = k_F C_e^{\frac{1}{n}} \qquad (7)$$

Freundlich:

$$q_e = q_m \frac{k_L \cdot C_e}{1 + k_L \cdot C_e} \qquad (8)$$

Tempkin:

$$q_e = k_T \ln f + k_t \ln C_e \qquad (9)$$

D-R:

$$\ln q_e = \ln q_m - \beta \varepsilon^2 \quad \varepsilon = RT \ln \left(1 + \frac{1}{C_e} \right) \quad E = \frac{1}{\sqrt{2\beta}} \qquad (10)$$

where q_m is the maximum adsorption capacity for Sr^{2+} of the sample, mg g^{-1}; k_L is the adsorption constant of the Langmuir model; k_F and $1/n$ are the adsorption constants of the Freundlich model; k_T and f are the constants of the Temkin model; k_T is related to adsorption heat; f is the maximum binding energy of adsorption; R is the molar gas constant, 8.3145 J (mol^{-1} L^{-1}); T is the absolute temperature, K; β is a constant related to the adsorption energy, mol^2 kJ^{-2}; ε is the Polanyi adsorption potential, KJ mol^{-1}; and E is the average free energy of adsorption, KJ mol^{-1}.
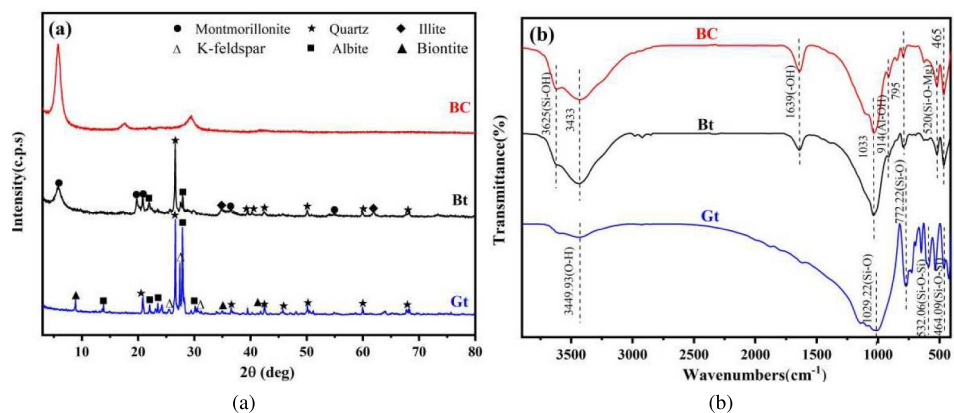
3 Results and discussion

3.1 Characterization

3.1.1 XRD and FT-IR

The mineral compositions of the samples were determined by XRD and FT-IR analyses.

Figure 2a shows the XRD patterns of the samples. The predominant mineral components of granite are quartz, albite, potassium feldspar, and biotite, with albite and K-feldspar together constituting approximately 70% of the mass percentage of the granite minerals. Bentonite contains montmorillonite as the main mineral component as well as secondary minerals, such as quartz, illite, and albite (Fig. 2b). The interplanar spacing of the bentonite colloid at the (001) plane differs slightly from that measured for the soil sample (1.52 nm). The diffraction curve of the bentonite colloid contains only a montmorillonite peak, indicating

Fig. 2 (Color online) XRD **a** and FT-IR **b** images of the sample

that secondary minerals were removed by centrifugation and dialysis [24]. The FT-IR analysis of the surface functional groups revealed that granite mainly consists of Si- and Al-based functional groups, including O–H, Si–O, Al–O, and Si–O–Si, which are similar to those present in bentonite [25, 26]. The bentonite colloids and bentonite have similar primary functional groups with minimal differences in the corresponding peak shapes and positions in the FT-IR spectra. This suggests that colloid formation has a negligible effect on the surface functional groups and chemical bonds of bentonite.

3.1.2 Zeta and particle size distribution

The zeta potential of the geological materials and bentonite colloids at different pHs is shown in Fig. 3a. Granite reaches the zero-point charge site at a pH of approximately 5.30, whereas bentonite and bentonite colloids have negative zeta potentials across the pH range of 3–11, with the bentonite colloids having a slightly lower potential than bentonite. The negative charge of bentonite arises from both the permanent charge of the structure and variable edge charge [27]. The colloid preparation process can affect the deprotonation of -SiOH and -AlOH, resulting in a bentonite colloid with a slightly lower potential than bentonite. However, the charges of bentonite and bentonite colloids were similar, indicating that the contribution from the edge charge was small. Figure 3b shows the average size and size distribution of the colloidal particles determined by dynamic light scattering. The colloidal particle sizes ranged from 100.9 to 433.5 nm with an average of 209.1 nm, suggesting relatively good colloidal stability. The polydispersity index (PDI) is a crucial parameter for characterizing particle size uniformity in a system. The bentonite colloid sample had a PDI of 0.217 in ultrapure water, indicating excellent dispersion.

3.1.3 SEM-EDS before and after adsorption

The TEM images of the samples are shown in Fig. 4. Granite exhibits a massive shape with a dense internal texture. Both bentonite and bentonite colloids display similar sheet morphologies with irregular edges, and the layered structure of
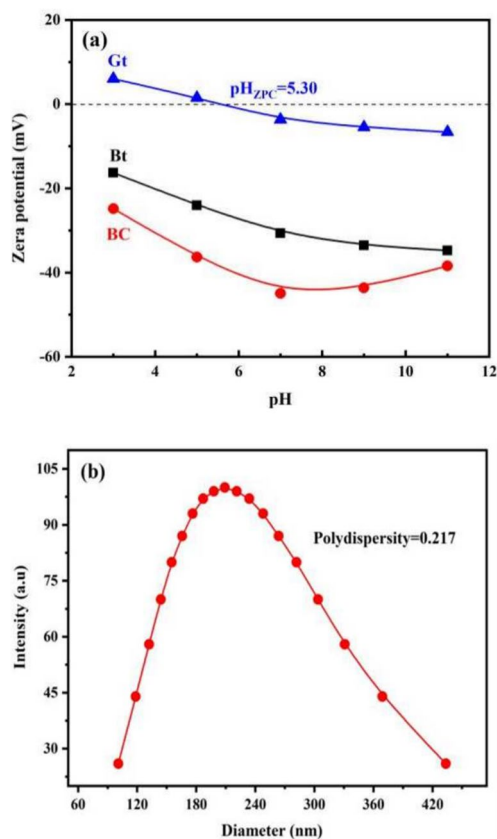

Fig. 3 (Color online) **a** Zeta potential of the sample; **b** particle size distribution of bentonite colloid
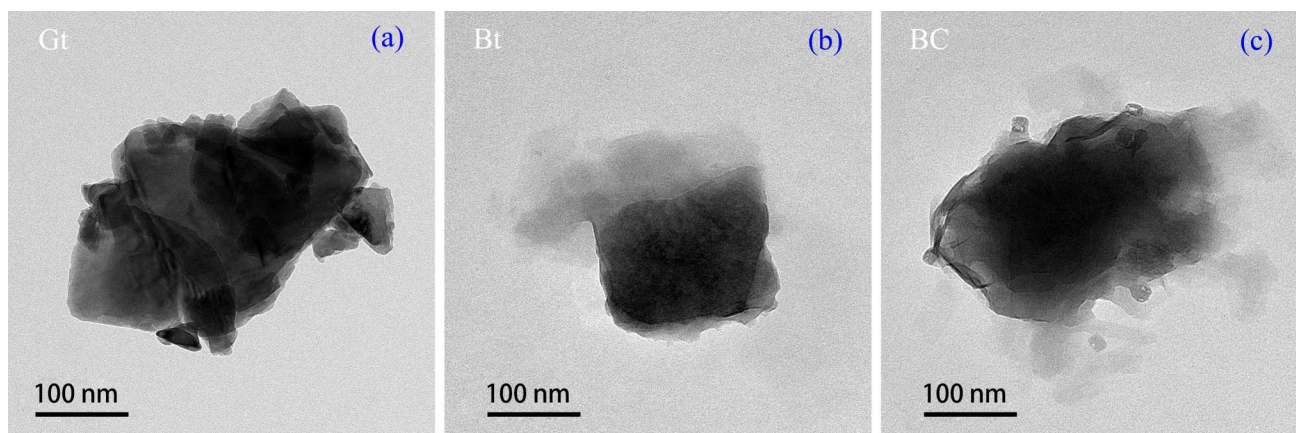

Fig. 4 TEM images of **a** granite, **b** bentonite, and **c** bentonite colloid

the colloid is more pronounced, confirming the XRD results. In addition, the TEM diagram illustrates that the prepared bentonite colloid has good dispersion, and the particle size of the colloid is approximately 200 nm, which is consistent with the particle size distribution test results of the colloid.

The surface morphologies of the samples before and after adsorption were characterized by SEM-EDS. Figure 5 shows that the granite samples have a fragmented distribution with unevenly sized layered fragments, and the sample surface is smooth with angular features. There is no significant difference in the morphology of the adsorbed granite before and after adsorption although adsorption makes the surface rougher and more fragmented, possibly because of immersion and agitation. The EDS results for the samples after adsorption indicate an increase in the quantity of adsorbed Sr^{2+} on the granite surface; however, there is no discernible distribution pattern for Sr^{2+} or a direct correlation between the distributions of Sr^{2+} and the other ions. The nonuniform particle size of bentonite indicates a distinct flaky structure with numerous irregular pores and cavities that facilitate the migration and diffusion of nuclides [28]. After adsorption,

the bentonite surface curls and becomes rough, presumably because adsorption is followed by drying [29].

The immersion and dialysis of bentonite generate bentonite colloids with a distinct layered morphology [30] with clearer boundaries and a more regular distribution than that of the soil samples. Adsorption does not change the morphology of the colloids considerably but makes the layered structure denser, more compact, and agglomerated, with less distinct interlayers. The EDS results presented in Fig. 6 show that O, Si, Al, and Mg are still the main elements in the colloidal samples after simulated nuclide adsorption. The Sr^{2+} ions are adsorbed unevenly on the colloids, mainly accumulating in the layered stacking regions, indicating the presence of different adsorption sites on the colloids, with the stacking edge sites having possibly a stronger affinity for Sr^{2+} [31]. The distribution of Sr on the colloids appears to be correlated with that of Ca, suggesting that Ca in the colloids might participate in the adsorption of Sr via an ion exchange reaction between Ca and Sr. Bentonite colloids primarily consist
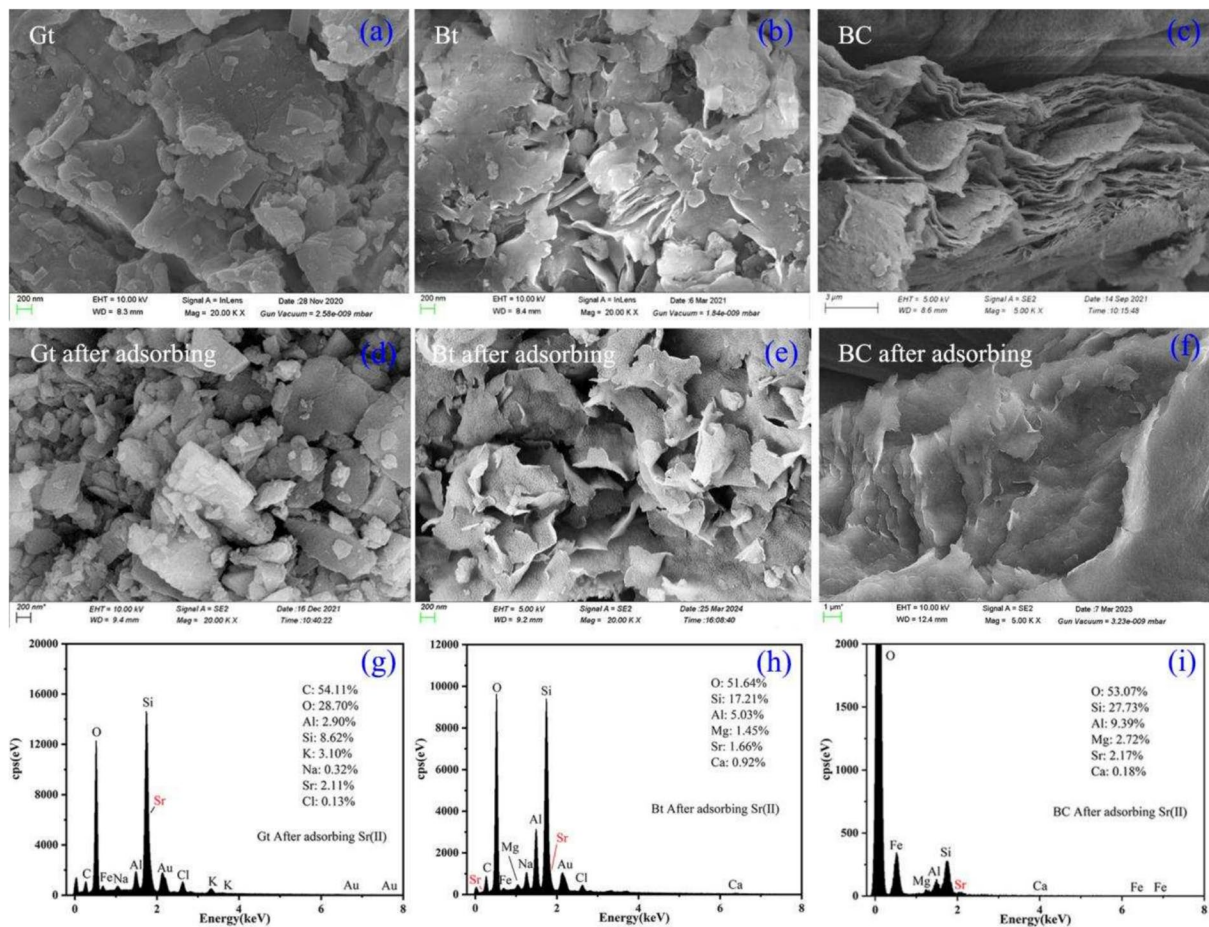

Fig. 5 SEM-EDS images of granite, bentonite, and bentonite colloid before and after adsorption
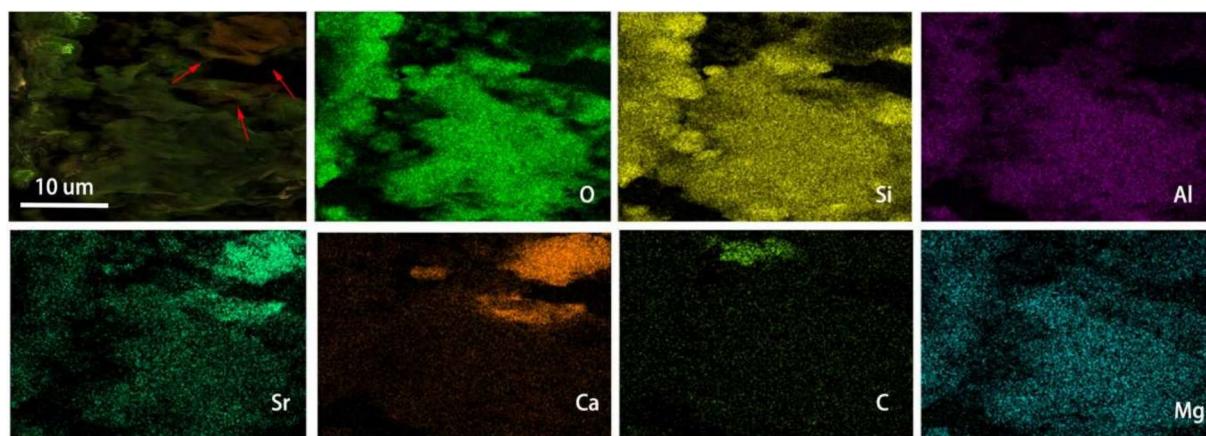
Fig. 6 (Color online) Distribution of various elements in adsorbed bentonite colloid

of montmorillonite. Missana et al. [32] observed similar phenomena for Sr adsorption onto Na-montmorillonite.

3.2 Adsorption behavior of Sr^{2+}

3.2.1 Adsorption kinetics

The results of the kinetic experiments are presented in Fig. 7. The adsorption capacities of the three geological materials for Sr^{2+} are observed to decrease in the order of bentonite colloid (BC)> bentonite (Bt)> granite (Gt). The adsorption equilibrium time for Sr^{2+} at five days is notably shorter for Gt than for BC and Bt, possibly because of the differences in the number and specificity of surface adsorption sites among the materials. The pseudo-second-order kinetic equation fits the adsorption data for Gt with a high correlation coefficient ($R^2 = 0.998$), suggesting that Sr^{2+} adsorption by Gt is primarily chemical [33]. The fitting curve for the Gt data based on the W-M model has three distinct regions corresponding to surface diffusion, internal diffusion, and equilibrium, indicating that intraparticle diffusion is not the sole rate-controlling step for Gt adsorption. In contrast, BC rapidly reaches adsorption equilibrium within 1 h, with q_e increasing from 2.136 mg/g to 13.989 mg/g, indicating a considerably greater adsorption capacity than that of Bt. This result is attributed to the larger specific surface area and lower surface charge of BC compared with that of Bt, leading to an increased number of adsorption sites and an enhanced ability to capture Sr^{2+} ions. Both BC and Bt data were most accurately fitted by pseudo-second-order kinetics, suggesting a chemical adsorption process involving surface complexation between functional groups and ion exchange [34]. Fitting the adsorption data of BC and Bt using the W-M equation revealed a two-stage process, unlike the adsorption on Gt. The fitted BC and Bt curves do not go through the origin,
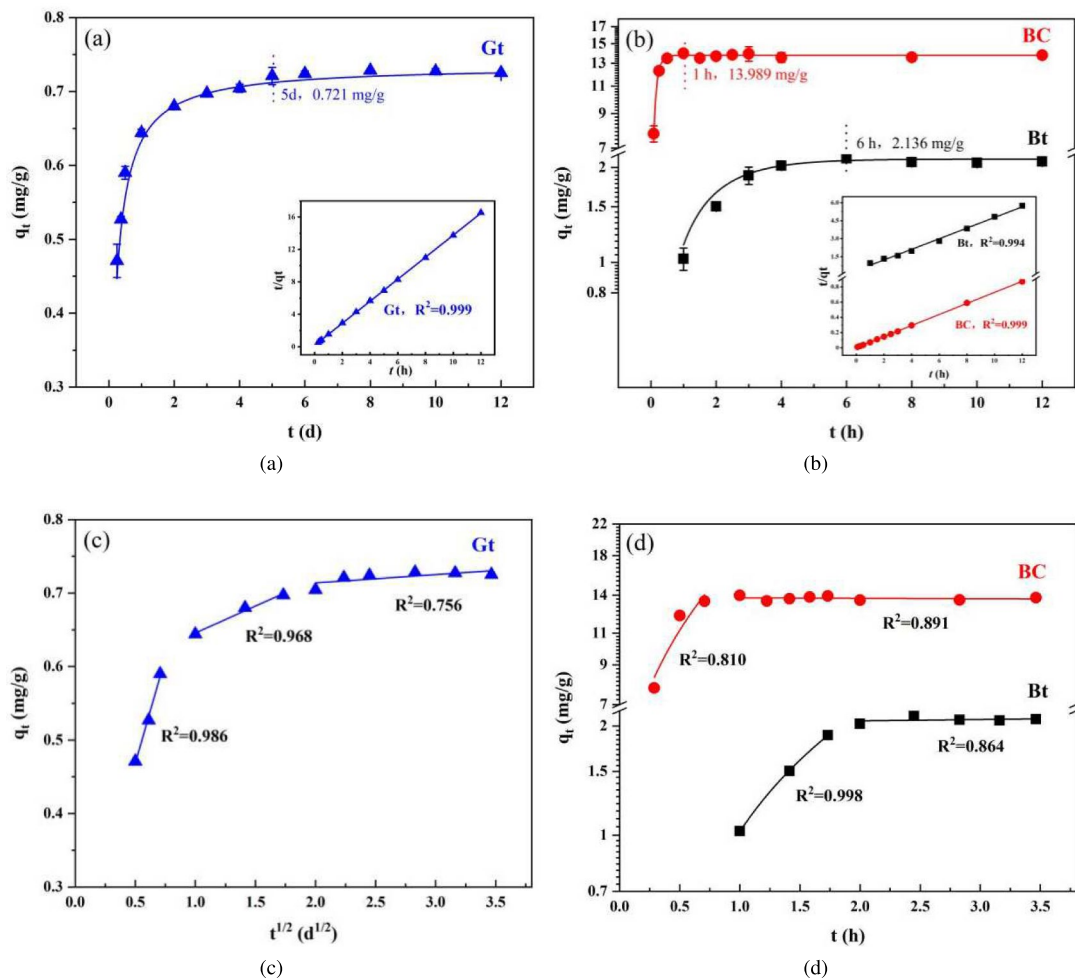
implying that the adsorption of Sr^{2+} is primarily determined by the adsorption sites and that the activation energy for adsorption and internal diffusion plays a minor role in the process [35]. Overall, the adsorption capacity of bentonite surpassed that of granite, suggesting a potential synergy between the two materials in blocking nuclide diffusion. However, the strong adsorption capabilities of bentonite colloids introduce considerable uncertainty and risk factors for the long-term disposal at repositories.

3.2.2 Effect of nuclide concentrations

The concentrations of nuclides carried in groundwater fluctuate with natural precipitation and water flow, which can deteriorate the blocking performance of barrier materials. Figure 8 shows that BC has the highest adsorption potential for Sr^{2+}, whereas the adsorption capacities of Gt, Bt, and BC for Sr^{2+} all increase with the Sr^{2+} concentration, gradually tending toward equilibrium. This phenomenon may be attributed to the low probability of Sr^{2+} binding to sites with low Sr^{2+} concentrations, with the probability increasing with Sr^{2+} concentration, which facilitates the capture of Sr^{2+} by adsorption sites. Consequently, the saturation of the binding sites decreases, resulting in a slower increase in the adsorption capacity, leading to gradual equilibrium [36]. To further explore the adsorption mechanism, we used the Langmuir, Freundlich, Temkin, and D-R isotherm models to fit the adsorption data at different Sr^{2+} concentrations (Table 3). Compared with the Freundlich and Temkin models, the fit of the Langmuir adsorption model to the Gt, Bt, and BC data had higher correlation coefficients of 0.996, 0.991, and 0.989, respectively. This indicates that Sr^{2+} is mainly adsorbed as a surface monolayer [37]. Within the experimental concentration range, the maximum adsorption capacities of Gt, Bt, and BC for Sr^{2+} were 1.229 mg/g, 4.407 mg/g,

Table 3 Adsorption data fitting kinetic equation and M-W equation parameters

Model	Material	Parameters		
Pseudo-first-order model	Gt	$q_e = 0.708$ mg/g	$k_1 = 3.838$ d^{-1}	$R^2 = 0.914$
	Bt	$q_e = 2.125$ mg/g	$k_1 = 0.763$ h^{-1}	$R^2 = 0.804$
	BC	$q_e = 13.088$ mg/g	$k_1 = 9.008$ h^{-1}	$R^2 = 0.957$
Pseudo-second-order model	Gt	$q_e = 0.736$ mg/g	$k_2 = 0.992$ g (mg d)$^{-1}$	$R^2 = 0.998$
	Bt	$q_e = 2.267$ mg/g	$k_2 = 0.560$ g (mg d)$^{-1}$	$R^2 = 0.993$
	BC	$q_e = 13.761$ mg/g	$k_2 = 3.941$ g (mg d)$^{-1}$	$R^2 = 0.999$
Weber-Morris model	Gt	$k_{id,1} = 0.223$ mg/g d$^{-1/2}$	$C_1 = 0.424$ mg/g	$R^2 = 0.986$
		$k_{id,2} = 0.048$ mg/g d$^{-1/2}$	$C_2 = 0.613$ mg/g	$R^2 = 0.968$
		$k_{id,3} = 0.001$ mg/g d$^{-1/2}$	$C_3 = 0.723$ mg/g	$R^2 = 0.756$
	Bt	$k_{id,1} = 1.174$ mg/g h$^{-1/2}$	$C_1 = -0.151$ mg/g	$R^2 = 0.998$
		$k_{id,2} = 0.017$ mg/g h$^{-1/2}$	$C_2 = 2.031$ mg/g	$R^2 = 0.891$
	BC	$k_{id,1} = 13.671$ mg/g h$^{-1/2}$	$C_1 = 4.369$ mg/g	$R^2 = 0.810$
		$k_{id,2} = -0.038$ mg/g h$^{-1/2}$	$C_2 = 13.814$ mg/g	$R^2 = 0.891$

(a)

(b)

(c)

(d)

Fig. 7 (Color online) Adsorption kinetics of **a** granite, **b** bentonite, and bentonite colloids. The illustration shows the linear fitting of quasi-second-order kinetics. Adsorption of **c** granite, **d** bentonite, and bentonite colloids fit using the W-M model ($T = 298$ K, pH $= 7$, $S/L_{Gt} = 20$ g/L, $S/L_{Bt} = 5$ g/L, $S/L_{BC} = 1$ g/L, $C_0 = 25$ mg/L)

and 30.303 mg/g, respectively, and were positively correlated with the specific surface areas of the materials. The fit

Table 4 Fitting isotherm model parameters for adsorption data at different concentrations

Models	Parameters	Values		
		Gt	Bt	BC
Langmuir	k_L	0.072	0.029	0.032
	q_m	1.257	6.750	43.360
	R^2	0.996	0.991	0.989
Freundlich	k_F	0.402	0.275	2.74
	$1/n$	0.194	0.671	0.573
	R^2	0.810	0.981	0.970
Tempkin	k_T	0.1928	1.331	8.645
	f	1.969	0.412	0.426
	R^2	0.901	0.986	0.987
D-R	β	0.0273	0.0389	0.0385
	E	25.901	18.17	18.366
	R^2	0.995	0.998	0.992

of the Gt, Bt, and BC data to the Temkin model also showed high linearity, suggesting strong intermolecular interactions between the adsorbent and adsorbate [38]. As the Freundlich constant, $1/n$, is less than 1, adsorption occurs easily. In the D-R equation, E denotes the energy required for 1 mol of nuclide to react with the adsorbent surface. Table 4 shows that Gt, Bt, and BC have E values above 16 kJ/mol; therefore, the adsorption mechanism of Gt, Bt, and BC is a chemical process [39], which is consistent with the kinetic fitting results.

3.2.3 Effect of pH

The pH of the environment strongly influences the mineral surface potential and species distribution of ions, which affects the adsorption of ions on minerals [40, 41]. Figure 9a shows the impact of the pH on Sr^{2+} adsorption. The adsorption of Sr^{2+} by Gt, Bt, and BC is impeded by both acidic and alkaline environments. The adsorption capacities of BC, Bt, and Gt peak at pH6 displaying amplitudes of 13.303 mg/g, 2.014 mg/g, and 0.733 mg/g, respectively.
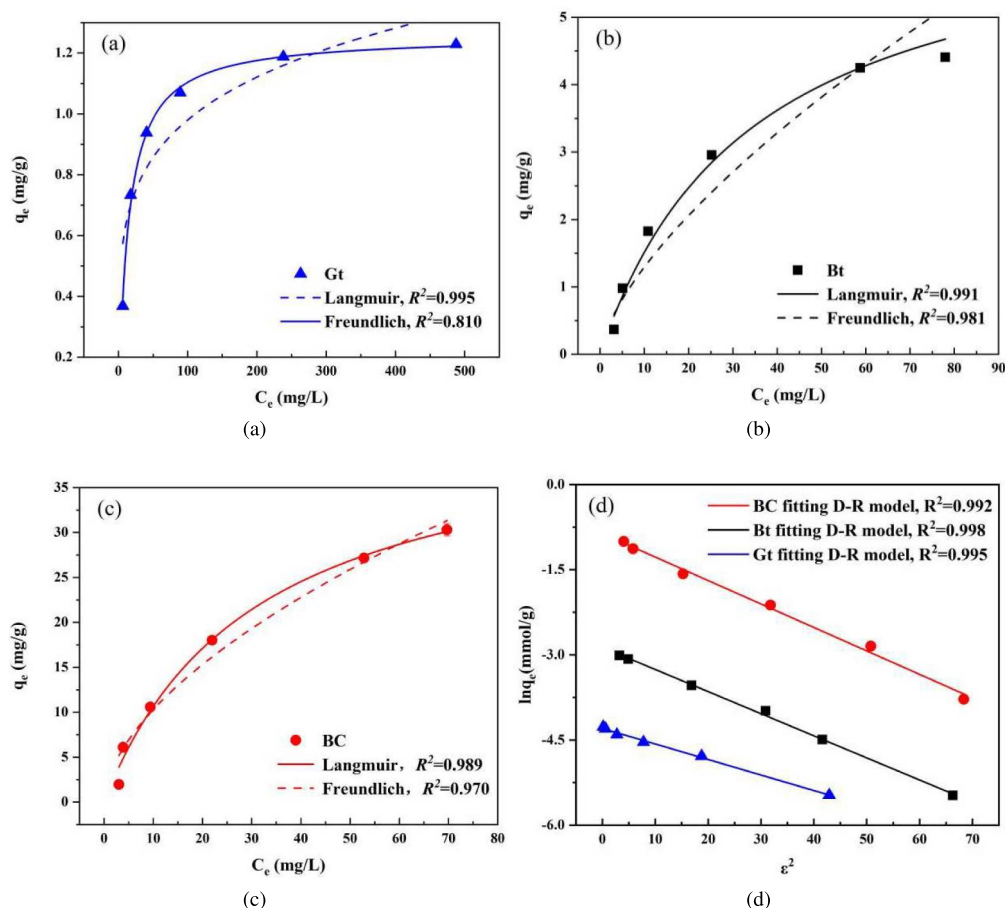

Fig. 8 (Color online) Adsorption isotherms of **a** granite, **b** bentonite, and **c** bentonite colloid. **d** Adsorption data fitted to the D-R isothermal model. ($T = 298$ K, pH = 7, $S/L_{Gt} = 20$ g/L, $S/L_{Bt} = 5$ g/L, $S/L_{BC} = 1$ g/L)
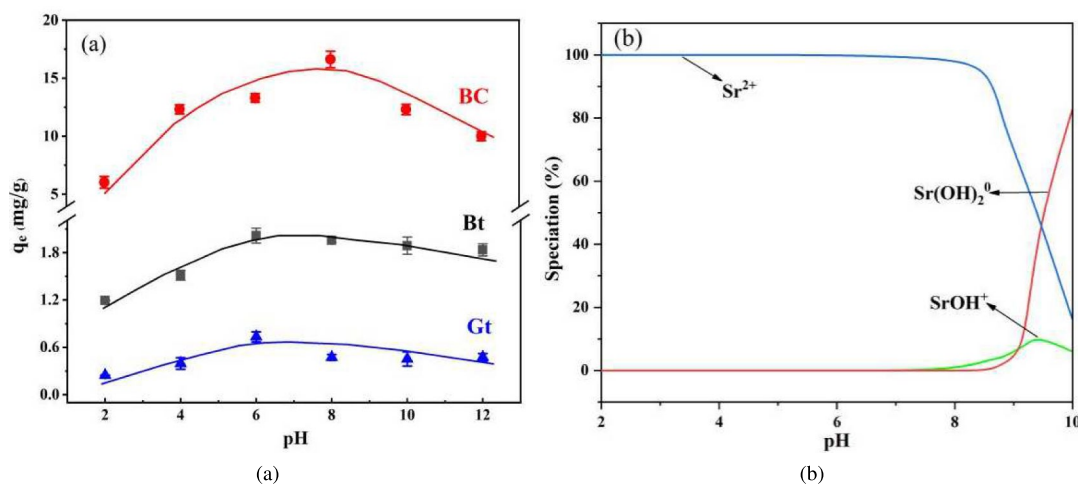
(a)   (b)

Fig. 9 (Color online) **a** Effect of pH on adsorption; **b** distribution of Sr species in pure water ($T = 298$ K, $S/L_{Gt} = 20$ g/L, $S/L_{Bt} = 5$ g/L, $S/L_{BC} = 1$ g/L)

This phenomenon may be attributed to the combined effects of the distribution of the strontium species, zeta potential, and colloidal stability. Figure 9b shows that Sr^{2+} is the primary strontium species under acidic conditions, where the competition between excess H^+ and Sr^{2+} for adsorption sites hinders adsorption [42]. Consequently, adsorption is generally inhibited in acidic environments. As the pH increases, complexes are formed between OH^- and Sr^{2+}, such as $Sr(OH)^+$ and $Sr(OH)^+$, which hinder adsorption. Therefore, the adsorption of Gt, Bt, and BC is impeded in alkaline environments. The poor stability of bentonite colloids in acidic environments results in a greater inhibitory effect on BC than on Gt or Bt [43, 44]. Zeta potential affects the affinity of the adsorbent for nuclides. The pH_{ZPC} value of Gt is approximately 5.30. At pHs below 5.30, the Gt surface is positively charged, which impedes the adsorption of Sr^{2+} via electrostatic repulsion. Conversely, at pHs > 5.30, the Gt surface becomes negatively charged, facilitating adsorption. Given that the permanent structural charge of Bt and BC is negative, the zeta potentials of these materials remain negative within the experimental pH range and decrease with increasing pH, indicating that the affinity of Bt and BC for Sr^{2+} increases with pH. However, this behavior does not alter the inhibition of adsorption by Bt and BC under alkaline conditions. This result can be explained in terms of the minor role that charge attraction plays in adsorption by Bt and BC. The pH of groundwater near disposal facilities is typically approximately 6.70. Around this pH, BC demonstrated high Sr^{2+} adsorption activity. Therefore, considering the potential effect of colloids on Sr^{2+} migration during disposal is important.

3.2.4 Effect of ions

The complex disposal environment for radioactive waste can result in a groundwater solution containing numerous ions that can affect the adsorption of nuclides by colloids and barrier materials. Preliminary analysis of the groundwater solution showed that the primary anions and cations in the groundwater near the disposal site were CO_3^{2-}, SO_4^{2-}, Fe^{3+}, Ca^{2+}, Mg^{2+}, and K^+. Given the potential of Sr^{2+} to form insoluble precipitates with anions such as CO_3^{2-} and SO_4^{2-} in groundwater, various electrolytes (KCl, $FeCl_3$, $CaCl_2$, and $MgCl_2$) have been used to investigate the adsorption behavior of Sr^{2+} in the presence of cations. Figure 10 shows that coexisting cations inhibit adsorption of Sr^{2+} by silicate minerals. These inhibitory effects were consistent for BC, Bt, and Gt, with the effectiveness decreasing in the order
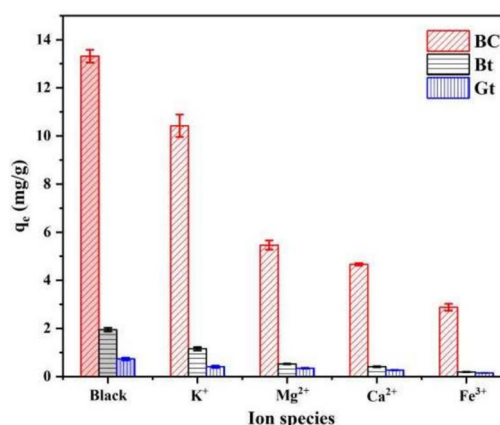

Fig. 10 (Color online) Effect of ions on adsorption at $T = 298\,K$, pH = 7, $S/L_{Gt} = 20$ g/L, $S/L_{Bt} = 5$ g/L, $S/L_{BC} = 1$ g/L, $C_{Sr} = 25$ mg/L, $C_{ion} = 0.01$ mol/L

$Fe^{3+} > Ca^{2+} > Mg^{2+} > K^{+}$. BC was inhibited the least because of its high unit adsorption capacity, whereas Gt displayed the most sensitivity to coexisting cations. Typically, high-valence cations compete more effectively for adsorption sites than low-valence cations [17], which accounts for Fe^{3+} having a more pronounced inhibitory effect than K^{+}. The difference between the inhibitory effects of Ca^{2+} and Mg^{2+} arises from the difference in the radii of the corresponding hydrated ions. The smaller the radius of a hydrated ion, the more strongly the ion competes with Sr^{2+} for adsorption. Given the same positive charge, the hydrated ion radius of Ca^{2+} (0.200 nm) is smaller than that of Mg^{2+} (0.310 nm), leading to a greater inhibitory effect for Ca^{2+} than Mg^{2+}.

3.3 Migration behavior of Sr^{2+}

3.3.1 Effect of bentonite colloid on migration

Batch adsorption experiments confirmed the robust adsorption capacity of BC for Sr^{2+}, motivating us to perform dynamic shower experiments to further investigate the influence of BC on Sr^{2+} migration in the granite system. Figure 11a shows a penetration curve in which neither the peak values of BC-Sr comigration nor Sr migration alone reaches 1, indicating retention of Sr^{2+} in the granite column. The longitudinal dispersion length (D_L) measured during Sr-BC comigration was 4.27×10^{-4}. Penetration of the granite column commenced at 18 h, which was considerably shorter than 70 h for Sr migration alone, indicating that the presence of colloids strongly promotes Sr^{2+} transport. This effect can be attributed to colloidal adsorption and inherent migration. Both bentonite colloids and granite exhibit negative charges

across a broad pH range, resulting in repulsion between the colloids and granite during nuclide transport. Static adsorption experiments revealed that the adsorption of Sr^{2+} by BC is robust, advancing BC as a carrier for accelerating Sr^{2+} transport. Many studies [30, 45–47] have corroborated that bentonite colloids strongly promote the migration of Em(III), Pu(IV), U(VI), and other nuclides.

Retention of Sr^{2+} in the granite column was observed in the migration experiments. To investigate the influence of colloids on Sr retention in granite, experiments were conducted on the adsorption/desorption of Sr^{2+} on BC and Gt. As shown in Fig. 11b, the adsorption results indicate that the BC-Gt system has strong adsorption capacity for Sr^{2+}. Under alkaline conditions, the adsorption capacity of the BC-Gt system is considerably greater than that of the Gt system because the stability of BC is enhanced in an alkaline environment [48]. The desorption experiments revealed that Gt has a lower adsorption capacity for Sr^{2+}, with most sites being reversible [49], which resulted in a low retention rate of (15.1% to 35.6%) for Sr^{2+} in Gt after desorption, which is consistent with the observations in the migration experiments. The retention of Sr^{2+} on Gt was slightly higher for the BC-Gt system, which is attributed to the small number of colloids attached to the surface of the granite. Notably, acidic conditions considerably increased Sr^{2+} retention, which can be attributed to the reduced stability of BC under acidic conditions [50], leading to sedimentation and adhesion with Gt, which weakens desorption. Overall, fractures in granite significantly increase the risk of Sr^{2+} leakage into the biosphere, and a small amount of colloid adhering to the surface of granite in the repository may slightly enhance the retention of Sr^{2+} in granite.
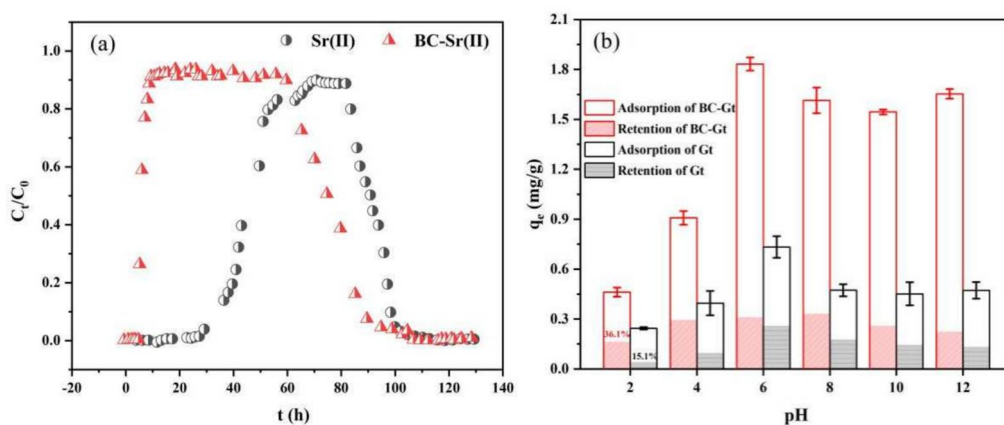

Fig. 11 (Color online) **a** Comigration curves of bentonite colloids and Sr^{2+}; **b** adsorption/desorption of Sr^{2+} by bentonite and granite (comigration: $T = 298$ K, pH = 7, $C_{BC} = 250$ mg/L, $C_{Sr} = 100$ mg/L, adsorption/desorption: $C_{Sr} = 50$ mg/L, $S/L_{Gt} = 20$ g/L, $S/L_{BC} = 0.2$ g/L)

However, colloid promotion was not observed to have a significant impact on the retention of Sr^{2+} in granite during dynamic migration experiments. This indicates that the influence of colloids on Sr^{2+} retention in granite should be considered alongside multiple factors such as flow rate, concentration, and pH, which are crucial for the safety assessment of nuclear waste disposal facilities.

3.3.2 Comigration of Bentonite Colloids and Polynuclides

As shown in Fig. 12b, the adsorption capacity of bentonite colloids for nuclides in multicomponent systems increased in the order of $Co^{2+} < Ni^{2+} < Sr^{2+} < Cs^+$, indicating that BC has the strongest affinity for Cs^+ in a multicomponent system. Analysis of the breakthrough curve revealed that the detection time for Sr^{2+} in the multinuclide comigration system surpassed that of the BC-Sr system. This delay may arise from the interaction between the numerous positively charged ions and bentonite colloids, mitigating electrostatic repulsion and reducing colloidal fluidity to promote bentonite agglomeration. These agglomerates were retained in the column because of size exclusion effects. Similar outcomes have been reported in studies on coexisting ions, in which fluctuations in ion content were attributed to external interference. In particular, the coexistence of ions with the same valence state causes steric hindrance, and filtering exerts more pronounced inhibitory effects on colloidal transport [51]. The effluent recovery rate increased in the order $Co^{2+} < Ni^{2+} < Sr^{2+} < Cs^+$ because of the nuclide adsorption capacity of BC. Nuclides adsorbed on BC can be retained in granite columns, diminishing the nuclide recovery rates in the effluent. Differences in affinities and binding capabilities of the

colloids and different simulated nuclides resulted in Sr^{2+} and Cs^+ eluting faster than Co^{2+}, which had a more pronounced elution curve. Nuclides with a stronger affinity for BC were affected more during migration. The penetration times of the nuclides in the multielement system increased in the order $Sr^{2+} < Cs^+ < Ni^{2+} < Co^{2+}$. Hence, considering the role of bentonite colloids in predicting Sr^{2+} migration is important in the safety assessment of repositories.

4 Conclusion

In this study, the impact of bentonite colloids on the migration of Sr^{2+} in granite was investigated in terms of adsorption capacity by conducting a combination of static adsorption and dynamic shower experiments. The influence of the multinuclide system on the migration of Sr^{2+} was analyzed. The findings of this study provide fundamental data and rational recommendations for safety assessment and establishment of migration models for nuclear waste disposal facilities. The results of the static adsorption experiments demonstrate that bentonite colloids have a considerably greater Sr^{2+} adsorption capacity than bentonite and granite, with maximum adsorption rates of 30.303 mg/g, 4.407 mg/g, and 1.2285 mg/g for bentonite colloids, bentonite, and granite, respectively. The adsorption behavior of Sr^{2+} conformed to both the Langmuir isotherm and pseudo-second-order kinetic models. Fitting the Sr^{2+} adsorption data with the W-M model revealed a two-stage distribution, indicating that single-layer chemical adsorption is controlled by the site activation energy. The distribution of Sr^{2+} on the colloid surface is nonuniform, and the mechanism of Sr^{2+} adsorption may involve ion exchange with Ca. Colloids have an optimal
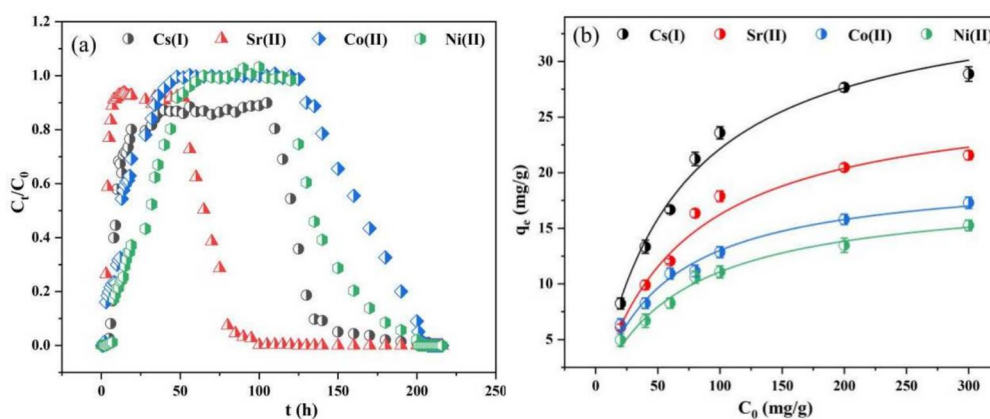

Fig. 12 (Color online) **a** Co-migration curves of bentonite colloids and polynuclides; **b** adsorption behavior of bentonite colloids on nuclides in polynuclides systems ($T = 298$ K, pH = 7, $C_{BC} = 250$ mg/L, $C_{nuclide} = 100$ mg/L)

Sr^{2+} adsorption capacity in neutral environments. However, cations in groundwater inhibit Sr^{2+} adsorption onto colloids, and the inhibition efficacy decreases in the following order: $Fe^{3+} > Ca^{2+} > Mg^{2+} > K^+$. Colloids maintain substantial adsorption potential even at high Sr^{2+} concentrations. Dynamic migration experiments revealed that the presence of colloids influences the retention of Sr^{2+} in granite, which is consistent with the findings of the adsorption/desorption experiments. However, the addition of colloids considerably accelerated the diffusion rate of Sr^{2+} in granite, reducing the penetration time from 70 h to 18 h. The presence of Co^{2+}, Ni^{2+}, and Cs^+ in a multinuclide system diminished the ability of the colloids to promote Sr^{2+} migration. The effluent recovery rate increased in the order $Co^{2+} < Ni^{2+} < Sr^{2+} < Cs^+$ because of the nuclide adsorption capacity of BC. This result confirms that the stronger the colloidal adsorption capacity for a nuclide, the greater is the impact of the colloids on Sr^{2+} migration. In conclusion, the presence of colloids increases the risk associated with Sr^{2+} migration in disposal facilities. Therefore, the influence of colloids on Sr^{2+} migration must be considered in safety assessments.

Declarations

Conflict of interest The authors declare that they have no competing interests.

References

1. Q. Jiang, Y.H. Wang, J.F. Cheng et al., Sorption of cesium on surrounding granite of Chinese low- and medium-level nuclear waste repository in the groundwater environment. J. Radioanal. Nucl. Ch. **5**, 331 (2022). https://doi.org/10.1007/s10967-022-08280-7

2. H. Liu, T. Fu, M.T. Sarwar et al., Recent progress in radionuclides adsorption by bentonite-based materials as ideal adsorbents and buffer/backfill materials. Appl. Clay Sci. **232**, 106796 (2023). https://doi.org/10.1016/j.clay.2022.106796

3. X. Zhang, F. Cai, F. Ma et al., Investigating the role of Na-bentonite colloids in facilitating Sr transport in granite minerals through column experiments and modeling. J. Hazard. Mater. **463**, 132851 (2024). https://doi.org/10.1016/j.jhazmat.2023.132851

4. T. Huang, D. Song, L. Zhou et al., Non-thermal plasma irradiated polyaluminum chloride for the heterogeneous adsorption enhancement of Cs^+ and Sr^{2+} in a binary system. J. Hazard. Mater. **424**, 127441 (2022). https://doi.org/10.1016/j.jhazmat. 2021.127441

5. T. Huang, S. Zhang, L. Zhou et al., Electrokinetics couples with the adsorption of activated carbon-supported hydroxycarbonate green rust that enhances the removal of Sr cations from the stock solution in batch and column. Sep. Purif. Technol. **265**, 118531 (2021). https://doi.org/10.1016/j.seppur.2021.118531

6. I.B. Rae, S. Pap, D. Svobodova et al., Comparison of sustainable biosorbents and ion-exchange resins to remove Sr^{2+} from simulant nuclear wastewater: batch, dynamic and mechanism studies. Sci. Total Environ. **650**, 2411–2422 (2019). https://doi.org/10.1016/j.scitotenv.2018.09.396

7. T. Missana, M. Garct'a-Gutiérrez, U. Alonso, Kinetics and irreversibility of cesium and uranium sorption onto bentonite colloids in deep granitic environments. Appl. Clay Sci. **26**(1), 37–150 (2004). https://doi.org/10.1016/j.clay.2003.09.008

8. F. Cai, F. Ma, X. Zhang et al., Investigating the influence of bentonite colloids on strontium sorption in granite under various hydrogeochemical conditions. Sci. Total Environ. **900**, 165819 (2023). https://doi.org/10.1016/j.scitotenv.2023.165819

9. Q. Tang, Z. Xu, Q. Tan et al., Insight into impact of phosphate on the cotransport and corelease of Eu(III)) with bentonite colloids in saturated quartz columns. J. Hazard. Mater. **461**, 132572 (2024). https://doi.org/10.1016/j.jhazmat.2023.132572

10. S. Zhu, Z. Tan, X. Wei et al., Interaction between Gaomiaozi bentonite colloid and uranium. Nuclear. Analysis **1**(4), 100048 (2022). https://doi.org/10.1016/j.nucana.2023.100048

11. B. Ghiasi, M.H. Niksokhan, A.M. Mazdeh et al., Co-transport of chromium(VI) and bentonite colloidal particles in water-saturated porous media: effect of colloid concentration, sand gradation, and flow velocity. J. Contam. Hydrol. **234**, 103682 (2020). https://doi.org/10.1016/j.jconhyd.2020.103682

12. Y. Sun, D. Pan, X. Wei et al., Insight into the stability and correlated transport of kaolinite colloid: effect of pH, electrolytes and humic substances. Environ. Pollut. **266**(2), 115189 (2020). https://doi.org/10.1016/j.envpol.2020.115189

13. H. Geckeis, T.S. Fer, W. Hauser et al., Results of the colloid and radionuclide retention experiment (CRR) at the Grimsel test site (GTS), Switzerland - impact of reaction kinetics and speciation on radionuclide migration. Radiochim. Acta **92**(9), 765–774 (2004). https://doi.org/10.1524/ract.92.9.765.54973

14. K. Kolomá, R. Červinka, I. Hanusová et al., ^{137}Cs transport in crushed granitic rock: the effect of bentonite colloids. Appl. Geochem. **96**, 55–61 (2018). https://doi.org/10.1016/j.colsurfa.2022.129636

15. S. Zhu, Y. Wang, C. Zheng et al., Gaomiaozi bentonite colloids: interactions with plutonium (IV) and zirconium (IV). Colloid. Surface. A. **650**, 129636 (2022). https://doi.org/10.1016/j.apgeochem.2019.01.015

16. O. Elo, P. Hölttä, P. Kekäläinen et al., Neptunium(V) transport in granitic rock: a laboratory scale study on the influence of bentonite colloids. Appl. Geochem. **103**, 31–39 (2019). https://doi.org/10.1016/j.jenvrad.2015.07.001

17. T.M. Dittrich, H. Boukhalfa, S.D. Ware et al., Laboratory investigation of the role of desorption kinetics on americium transport associated with bentonite colloids. J. Environ. Radioact. **148**, 170–182 (2015). https://doi.org/10.1080/00295450.2022.2083749

18. Y.H. Wang, Q. Jiang, Y.X. Yang et al., Adsorption properties of Cs(I) and Co(II) on GMZ bentonite colloids. Nucl. Technol. **208**(12), 1894–1907 (2022). https://doi.org/10.1080/00295450.2022.2083749

19. H. Wu, Z. Xu, L. Zhu et al., Adsorption of strontium at K-feldspar-water interface. Appl. Radiat. Isot. **181**, 110111 (2022). https://doi.org/10.1016/j.apradiso.2022.110111

20. T. Huang, D. Song, C. Yang, Nonthermal plasma-irradiated polyvalent ferromanganese binary hydro(oxide) for the removal of uranyl ions from wastewater. Environ. Res. **217**, 114911 (2023). https://doi.org/10.1016/j.envres.2022.114911

21. M. Yilmaz, T.J. Al-MusawiM, K. Saloot, Synthesis of activated carbon from Lemna minor plant and magnetized with iron (III) oxide magnetic nanoparticles and its application in the removal of ciprofloxacin. Biomass. Convers. Bior. **14**(1), 649–662 (2024). https://doi.org/10.1007/s13399-021-02279-y

22. H.W. Ayoob, A.M. Ridha, A.A. Jassim et al., Enhanced adsorption of phenol using graphene oxide-bentonite nanocomposites: synthesis, characterisation, and optimisation. J. Mol. Liq. **395**, 123833 (2024). https://doi.org/10.1016/j.molliq.2023.123833

23. T. Huang, Z. Su, Y. Dai et al., Enhancement of the heterogeneous adsorption and incorporation of Uraniumvi caused by the intercalation of β-cyclodextrin into the green rust. Environ. Pollut. **290**, 118002 (2021). https://doi.org/10.1016/j.envpol.2021.118002

24. P. Borralleras, I. Segura, M.A.G. Aranda et al., Influence of experimental procedure on d-spacing measurement by XRD of montmorillonite clay pastes containing pce-based superplasticizer. Cem. Concr. Res. **116**, 266 (2019). https://doi.org/10.1016/j.cemconres.2018.11.015

25. H. Li, B. He, P. Li et al., Adsorption behaviors of Eu(III) on granite: batch, electron probe micro-analysis and modeling studies. Environ. Earth Sci. **78**(8), 1–9 (2019). https://doi.org/10.1007/s12665-019-8170-y

26. C.L. Wang, X.Y. Yang, C. Li et al., The sorption interactions of humic acid onto Beishan granite. Colloid. Surface. A. **484**, 37–46 (2015). https://doi.org/10.1016/j.colsurfa.2015.07.045

27. Z. Xu, Y.L. Sun, Z.W. Niu et al., Kinetic determination of sedimentation for GMZ bentonite colloids in aqueous solution: effect of pH, temperature and electrolyte concentration. Appl. Clay Sci. **184**, 105393 (2020). https://doi.org/10.1016/j.clay.2019.105393

28. R. Zuo, Z.R. Xu, X. Wang et al., Adsorption characteristics of strontium by bentonite colloids acting on claystone of candidate high-level radioactive waste geological disposalsites. Environ. Res. **213**, 113633 (2022). https://doi.org/10.1016/j.clay.2019.105393

29. P.M. Fox, R.M. Tinnacher, M.C. Cheshire et al., Effects of bentonite heating on U(VI) adsorption. Appl. Geochem. **109**, 104392 (2019). https://doi.org/10.1016/j.apgeochem.2019.104392

30. K.K. Norrfors, R. Marsac, M. Bouby et al., Montmorillonite colloids: II. Dependence of colloidal size on radionuclide adsorption. Appl. Clay Sci. **123**, 292–303 (2016). https://doi.org/10.1016/j.clay.2016.01.017

31. K.K. Norrfors, M. Bouby, S. Heck et al., Montmorillonite colloids: I. characterization and stability of dispersions with different size fractions. Clay. Sci. **114**, 179–189 (2015). https://doi.org/10.1016/j.clay.2015.05.028

32. T. Missana, M. Garct'a-Gutiérrez, Adsorption of bivalent ions (Ca(II), Sr(II), and Co(II)) onto febex bentonite. Phys. Chem. Earth. **32**(8), 559–567 (2007). https://doi.org/10.1016/j.pce.2006.02.052

33. Z. Sun, Y.G. Chen, X. Mu et al., Graphene oxide-modified organic Gaomiaozi bentonite for Yb(III) adsorption from aqueous solutions. Mater. Chem. Phys. **274**, 125176 (2021). https://doi.org/10.1016/j.matchemphys.2021.125176

34. S. Song, S. Huang, R. Zhang et al., removal of u(vi) and humic acid on defective TiO_2-X investigated by batch and spectroscopy techniques. Chem. Eng. **325**, 576–587 (2017). https://doi.org/10.1016/j.cej.2017.05.125

35. C.L. Chen, X.L. Li, D.L. Zhao et al., Adsorption kinetic, thermodynamic and desorption studies of Th(IV) on oxidized multi-wall carbon nanotubes. Colloid. Surface. A. **302**, 449–454 (2007). https://doi.org/10.1016/j.colsurfa.2007.03.007

36. A.Y. Ahmad, M.A. AlGhouti, M. Khraisheh et al., Insights into the removal of lithium and molybdenum from groundwater by adsorption onto activated carbon, bentonite, roasted date pits, and modified-roasted date pits. Bioresour. Technol. Rep. **18**, 101045 (2022). https://doi.org/10.1016/j.biteb.2022.101045

37. E.A. Alabbad, Effect of direct yellow 50 removal from an aqueous solution using nano bentonite; Adsorption isotherm, kinetic analysis, and thermodynamic behavior. Arab. J. Chem. **16**(2), 104517 (2022). https://doi.org/10.1016/j.arabjc.2022.104517

38. J.J. Wang, X.Y. Li, Y. Fang et al., Efficient adsorption of tetracycline from aqueous solution using copper and zinc oxides modified porous boron nitride adsorbent. Coll. Surf. A. **666**, 131372 (2023). https://doi.org/10.1016/j.colsurfa.2023.131372

39. L. Popoola, Tetracycline and sulfamethoxazole adsorption onto nanomagnetic walnut shell-rice husk: isotherm, kinetic, mechanistic, and thermodynamic studies. Int. J. Environ. Anal. Chem. **100**, 1–23 (2019). https://doi.org/10.1080/03067319.2019.1646739

40. L.A. Attar, B. Safia, B.A. Ghani, Uptake of ^{137}Cs and ^{85}Sr into thermally treated bentonite. J. Environ. Radioact. **193**, 36–43 (2018). https://doi.org/10.1016/j.jenvrad.2018.08.015

41. T. Huang, L.W. Pan, J.C. Dong et al., A comprehensive investigation of zeolite-rich tuff functionalized with 3-mercaptopropionic acid intercalated green rust for the efficient Remval of Hg(II) and Cr(VI) in a binary system. J. Environ. Manage. **324**, 116344 (2022). https://doi.org/10.1016/j.jenvman.2022.116344

42. D.H. Xu, R. Zuo, K. Han et al., Sorption of Sr in granite under typical colloidal action. J. Contam. Hydrol. **233**, 103659 (2020). https://doi.org/10.1016/j.jconhyd.2020.103659

43. E. Tombácz, M. Szekeres, Colloidal behavior of aqueous montmorillonite suspensions: specific role of pH in the presence of different electrolytes. Appl. Clay Sci. **27**(1/2), 79–95 (2004). https://doi.org/10.1016/j.clay.2004.01.001

44. M.H. Baik, S.Y. Lee, Colloidal stability of bentonite clay considering surface charge properties as a function of pH and ionic strength. J. Ind. Eng. Chem. **16**(5), 837–841 (2010). https://doi.org/10.1016/j.jiec.2010.05.002

45. H. Movahedi, K. Shaygan, N. Bovet et al., Fate and cotransport of Pb(II) and Cd(II) heavy ions with bentonite colloidal flow in saturated porous media: The role of filter cake, counterions, colloid concentration, and fluid velocity. J. Hazard. Mater. **466**, 133546 (2024). https://doi.org/10.1016/j.jhazmat.2024.133546

46. E.L. Tran, N. Teutsch, O. Klein-BenDavid et al., Uranium and cesium sorption to bentonite colloids under carbonate-rich environments: Implications for radionuclide transport. Sci. Total Environ. **643**, 260–269 (2018). https://doi.org/10.1016/j.scitotenv.2018.06.162

47. Y. Chen, Y. Li, Q. Tian et al., Bentonite colloids mediated Eu(III) migration in homogeneous and heterogeneous media of Beishan granite and fracture-filling materials. Sci. Total Environ. **904**, 166731 (2023). https://doi.org/10.1016/j.scitotenv.2023.166731

48. J. Xiao, Y.T. Chen, W.H. Zhao et al., Sorption behavior of U(VI) onto Chinese bentonite: effect of pH, ionic strength, temperature and Humic acid. J. Mol. Liq. **188**, 178–185 (2013). https://doi.org/10.1016/j.molliq.2013.10.008

49. J.Z. Zang, J. Wang, X. Han et al., Sorption and desorption of Sr onto a rough single fractured granite. J. Contam. Hydrol. **228**, 103558 (2019). https://doi.org/10.1016/j.jconhyd.2019.103558

50. Z. Xu, D. Pan, Y.L. Sun et al., Stability of GMZ bentonite colloids: aggregation kinetic and reversibility study. Appl. Clay Sci. **161**, 436–443 (2018). https://doi.org/10.1016/j.clay.2018.05.002

51. A. Sdiri, T. Higashi, R. Chaabouni et al., Competitive removal of heavy metals from aqueous solutions by montmorillonitic and calcareous clays. Water Air Soil Pollut. **223**, 1191–1204 (2012). https://doi.org/10.1007/s11270-011-0937-z